DE GRUYTER DOI 10.1515/zpch-2014-0480 — Z. Phys. Chem. 2014; 228(4–5): 337–350

Philipp Gruene, Burkhard Butschke, Jonathan T. Lyon, David M. Rayner, and André Fielicke*

Far-IR Spectra of Small Neutral Gold Clusters in the Gas Phase

Abstract: Vibrational spectra of small neutral gold clusters containing up to 8 Au atoms are measured in the far-infrared ($46-222\ cm^{-1}$) *via* photodissociation of their complexes with krypton atoms. Comparisons with calculated IR spectra for bare Au_n clusters using density functional theory allow for structural assignment. For these small sizes, all clusters are found to be planar and of comparably high symmetry. For Au_6 no data is available, as this cluster size is not detected in the photoionization mass spectra due to its high ionization energy. The structures assigned are for $n = 4$: rhombus (D_{2h}); 5: trapezoid (C_{2v}); 7: edge-capped triangle (C_s), 8: 4-fold edge-capped square (D_{4h}).

Keywords: Vibrational Spectroscopy, Metal Clusters, Structure Determination, Multiple Photon Dissociation, Far-Infrared.

***Corresponding Author: André Fielicke,** Institut für Optik und Atomare Physik, Technische Universität Berlin, Hardenbergstr. 36, D-10623 Berlin, Germany, e-mail: fielicke@physik.tu-berlin.de

Philipp Gruene, Burkhard Butschke, Jonathan T. Lyon, André Fielicke: Fritz-Haber-Institut der Max-Planck-Gesellschaft, Faradayweg 4-6, D-14195 Berlin, Germany

Burkhard Butschke: present address: Department of Organic Chemistry, Weizmann Institute of Science, 76100 Rehovot, Israel

Jonathan T. Lyon: Department of Natural Sciences, Clayton State University, 2000 Clayton State Blvd., Morrow, Georgia 30260, USA

David M. Rayner: National Research Council, 100 Sussex Drive, Ottawa, Ontario, Canada K1A OR6

Dedicated to: Professor Klaus Rademann on the occasion of his 60th birthday

1 Introduction

Detailed knowledge of the geometric and electronic structures of clusters is a prerequisite for understanding the evolution of their properties with size. This is particularly the case for systems where novel non-bulk like properties emerge at the nano-scale. Examples for such observations are the transition to insulator or even van-der-Waals bound clusters for certain metals [1, 2], the optical properties of

metal clusters or nano-particles embedded in glass [3, 4], or the appearance of unprecedented chemical reactivity below a particular particle size. The discovery of high catalytic activity of gold nano-particles for low temperature CO oxidation [5] likewise has triggered many investigations of the physical and chemical properties of gas-phase gold clusters including their structures [6–9].

Most experimental investigations sensitive to structural details of gold clusters have been performed on charged species due to the possibility of easy mass separation and thereby size-selection. These studies give insight into an interesting structural evolution that does not have a direct parallel in other metals: the transition from 2- to 3-dimensional structures at comparably large sizes [7, 8]. For the cationic clusters, the smallest cluster with a 3D geometry is Au_8, while for the anions one finds the crossover at the 12-atom cluster with co-existing 2D and 3D structures. For neutral clusters one might intuitively expect the transition to occur somewhere in between. The only experimentally confirmed structures are those of Au_4, Au_7 (2D) and Au_{19}, Au_{20} (3D) [10, 11], leaving a large unexplored gap. There have been many theoretical studies addressing this topic. For the neutrals, the small sizes are found to be planar [12–19]. In contrast to what can be inferred from the studies on the ions, there have been some predictions that the dimensionality change for the neutrals may occur at or even below Au_8 [20–22]. It is evident, however, that the transition size as well as the predicted ground state structures, highly depend on the theoretical methods and how they treat relativistic effects and dispersion interactions. Several studies have explicitly focussed on Au_8, and in particular more recent CCSD(T) calculations using comparably large basis sets find a 2D configuration as ground state for Au_8, while the energy differences to the lowest 3D structure are only small [23–28].

There are only few direct experimental studies on neutral gold clusters in the gas phase. Their ionization potentials have been determined by threshold electron impact ionization [29], excited states of Au_3 have been characterized *via* resonant two-photon ionization spectroscopy [30], and for the same size, a vibronic spectrum in the mid-IR has been measured in a Ne matrix [31]. Optical spectra of odd-sized clusters Au_n (n = 7, 9, 11, 13) have been measured using photodissociation of weakly bound complexes with Xe atoms [32] as well as for mass-selectively deposited small (n = 1–5, 7–9) Au clusters in Ne matrices [33]. The latter results have been compared to results of TD-DFT calculations that reproduce several experimental features, but do not allow with certainty the attribution of the measured spectra to specific isomers. Vibrational data for neutral gold clusters as formed *via* electron detachment from the anions have been obtained *via* vibrationally resolved photoelectron spectroscopy [34–37]. It is, however, not clear that these are the ground state structures of the neu-

trals, taken the charge state dependence of the gold-cluster structures into account. By using slow-electron velocity-map imaging (SEVI) [38], transitions to single vibrational levels of Au_2 and Au_4 have been recently observed [39, 40]. We have used photodissociation of rare-gas complexes to obtain the vibrational spectra in the far-IR [10, 11]. In combination with quantum chemical calculations, such vibrational spectra can give detailed structural information for metal clusters.

In the following we report experimental far-IR spectra for neutral gold clusters up to Au_8. While the spectra for $n = 3$, 4, and 7 have been discussed before [10, 11], we now include Au_5 and Au_8. No experimental data is available for Au_6 because it is not detected due to its high ionization energy. We compare IR multiple photon dissociation (IR-MPD) spectra of the Au_nKr_m complexes with calculated harmonic IR spectra obtained using density functional theory (DFT) for the *bare* clusters Au_n. It will be shown that for the species discussed here, this is sufficient for the determination of the gold cluster structures. A detailed discussion of the effects of rare-gas ligands and anharmonicity (i.e. through finite temperature effects and fluctionality) has been given elsewhere for $n = 3$, 4, 7 [11].

2 Methods

2.1 Experimental

The experiments are performed in a molecular beam machine (see Figure 1) connected to a beamline of the Free Electron Laser for Infrared eXperiments (FELIX) [41]. The set-up is a different one than used in most of our earlier experiments on metal clusters [42, 43], implementing a continuous gas expansion laser ablation source. This is essential to form a stable distribution of Au_n-Kr complexes. The set-up follows the design of Campargue [44] with a moderate vacuum (0.1 mbar) in the source chamber obtained by a mechanical booster/rotary vane pump combination (Edwards EH1200/E2M80), differential pumping stage (10^{-4} mbar), and a high vacuum stage (10^{-6} mbar) that contains a reflectron time-of-flight mass spectrometer (Jordan TOF Products, Inc.); the latter two are pumped by turbomolecular pumps.

Gold clusters are produced by pulsed (10 Hz) laser ablation of a solid gold target in a continuous stream of a carrier gas, consisting of 1.5% krypton in helium. The total gas flow was about 1600 sccm, leading to a stagnation pressure of ~ 10 mbar in the source channel. The complete cluster source [45] is cooled to ~ 100 K by liquid nitrogen flowing continuously through the tubing soldered

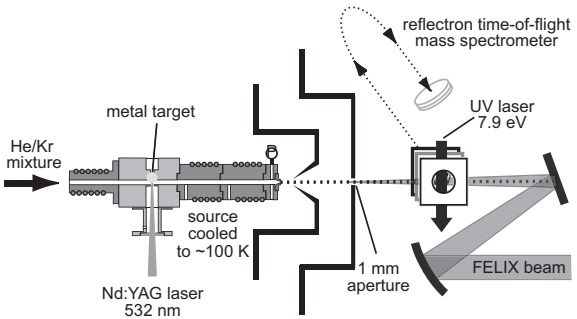

Figure 1: Experimental set-up for far-IR multiple photon dissociation spectroscopy of neutral gold cluster–krypton complexes.

onto the copper extensions of the central source part where ablation occurs. The clusters are efficiently thermalized in the source and weakly bound complexes with Kr atoms are formed. The cluster beam emitted by the source is skimmed and passes through a 1 mm diameter circular aperture. Neutral clusters are photoionized by 7.9 eV photons from an F_2 laser. The aperture defines the overlap between the cluster beam and the counter-propagating IR laser beam from FELIX. The ionization laser is timed to ionize the cluster package that has been irradiated with the ~ 10 μs long IR pulse while flying through the weak focus close to the aperture. This corresponds to a delay between IR and UV pulses of approximately 50 μs.

For a given IR wavenumber typically 600–1000 single mass spectra are averaged and the same number of reference mass spectra, with the IR laser off, are taken on alternating shots. The IR laser is tuned between 46 and 222 cm^{-1}, typical pulse energies are on the order of 20–40 mJ, and the bandwidth of the IR radiation is about 1%–2% of the central wavelength. Size-specific far-IR spectra of the neutral cluster species are obtained by monitoring the IR induced changes in the intensity of the cations I^+. The relative intensity changes of the ionized species $I^+(\nu)/I_0^+$ are evaluated as a function of wavenumber ν. As the ionization yield of a particular cluster species I^+/I^{neut} is constant as long as saturation effects are avoided this equals the relative change in the neutral species. Relative absorption cross sections are calculated using:

$$\sigma(\nu) = -\ln[I^+(\nu)/I_0^+]/F(\nu).$$

The normalization with the IR photon fluence $F(\nu)$ accounts for its variations over the tuning range. More technical details on far-IR multiple photon dissociation of metal cluster–rare gas complexes have been given before [42, 43].

2.2 Theoretical

For comparison with the experimental spectra, IR spectra are calculated for the various low-energy isomers of the pure Au_n clusters that have been suggested in the literature [12–28]. Computations are performed within TURBOMOLE V6.4 [46] using density functional theory employing the def2-TZVP basis set (with the associated effective core potential def2-ecp) [47] and the Tao–Perdew–Staroverov–Scuseria meta-GGA functional [48]. The suitability of such type of functionals for the investigation of gold clusters has been discussed before [49, 50].

The calculated harmonic vibrational frequencies are uniformly scaled by a constant multiplication factor of 1.06 that is chosen based on the comparison of experimental and theoretical peak positions for the gold clusters. Scaling of the calculated (harmonic) vibrational frequencies is performed to compensate for the anharmonicity of the vibrations, the neglect of electron correlation, or the use of incomplete basis sets [51]. Therefore, the optimal vibrational scaling factors depend on details of the theoretical methods [52]. Scaling factors larger than 1 we encounter also in studies of other systems, like pure and doped Si clusters [53, 54] and we attribute their need to a systematic underestimation of the calculated bond strength, due to shortcomings in our DFT approach.

3 Results and discussion

3.1 Ionization efficiencies of Au_nKr_m

Figure 2 shows mass spectra obtained by single photon ionization of the neutral cluster distribution at 7.9 eV. The observed intensity pattern for Au_n^+ follows a strong odd/even oscillation with intense signals for the odd sized clusters and no or very little signals for $n = 4, 6, 8$, while Kr complexes are observed for all sizes except $n = 6$. From $n = 9$ on, all bare gold clusters and the Kr complexes are efficiently ionized. For the bare clusters, this follows largely the known experimental vertical ionization energies that had been determined *via* threshold electron impact ionization [29].

The Kr complexes are expected to have a lower ionization energy (IE) compared to the bare clusters by approximately the strength of the charge-induced dipole interaction in the cationic Au_nKr^+ complex [55]. The precise interaction energy will depend on the structure of the charged metal cluster, but can be approximated to be on the order of 0.2 eV per Kr atom. This brings the IE of Au_4Kr_2 and $Au_8Kr_{2/3}$ into the range of the photon energy of the ionization laser. The IE of

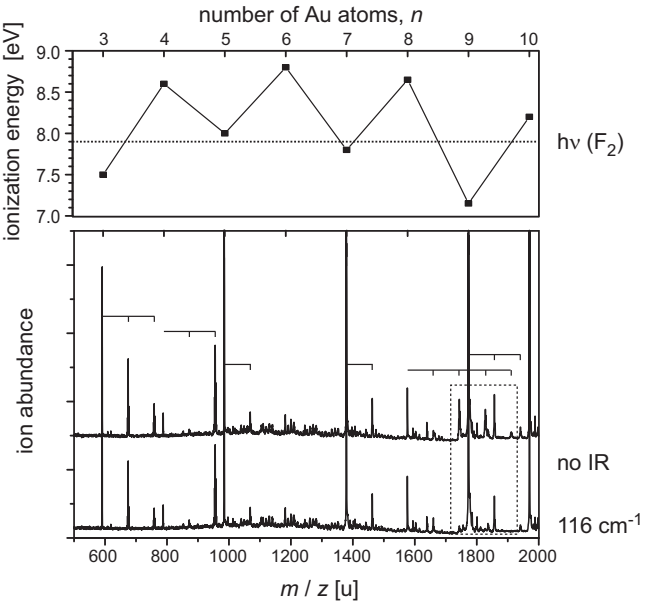

Figure 2: Mass spectra of Au_nKr complexes ionized with 7.9 eV photons (bottom) compared to the ionization energies of bare Au_n clusters (top). The bars mark the sequences of bare clusters and the corresponding Kr complexes. The upper mass spectrum is taken without IR irradiation, while for the lower one the IR is tuned to a resonance in the Au_8Kr_n complexes that are depleted (see the marked mass range). Ionization of residual pump oil leads to some background signal in the 1000–1500 u range.

Au_6, 8.8 eV, is the highest for all clusters in the investigated size range and neither the ionization of the bare clusters nor its Kr complexes are observed. The small intensities observed for bare Au_4^+ and Au_8^+ might be due to a hot fraction of neutral clusters. They are not due to fragmentation of the ionized Kr complexes, as their intensity does not depend on the IR wavelength.

3.2 Far-IR spectra

Multiple photon dissociation spectra are recorded in the 46–222 cm^{-1} range. The lower limit was given by the performance of FELIX, while at higher frequencies no fundamental vibrations of the gold clusters are expected. This is in agreement with the predicted vibrational frequencies, see below. Note, for the neutral dimer ω_e is 190.9 cm^{-1} [52] and only very few bands are observed above this value for the higher clusters (Figure 3). The spectra of the different cluster sizes are rather dis-

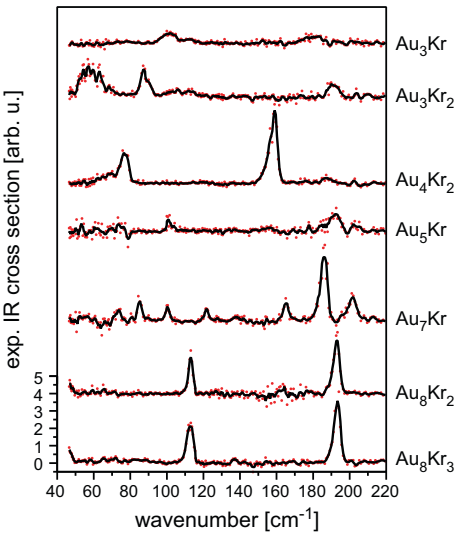

Figure 3: IR-MPD spectra of krypton complexes of Au_3-Au_8. The dots are the measured data points, the lines are their 5-point running average. The spectra are all plotted on the same intensity scale and offset for clarity.

similar, demonstrating that they are fingerprints of the clusters' individual structures. The very similar appearance of the spectra of Au_8Kr_2 and Au_8Kr_3 illustrates that the addition of Kr atoms has no significant effect on the spectra. The case of Au_3Kr/Au_3Kr_2, where the spectra differ considerably, is somehow special, as the Kr atoms are comparatively strongly bound to Au_3 and lead to a change from a slightly obtuse (in Au_3Kr) to an acute (in Au_3Kr_2) geometry; furthermore the presence and position of the bands is affected by anharmonic effects. This observation has been discussed in detail elsewhere [11], and the experimental spectra are only included here for completeness.

3.3 Au_4

For the tetramer, only the complex with two Kr atoms is observed in the mass spectrum. Its IR spectrum fits the predictions for the rhombic isomer **4a** well, both in terms of band position and relative intensities (Figure 4). The Y-shaped isomer **4b** is found to be isoenergetic at the level of theory used here, but experimentally, there are no signs of any contribution to the spectrum. However, it has been predicted that **4b** has a higher ionization potential than **4a** [11, 18], and its complexes (if present) may not get ionized by the F_2 laser. The observed

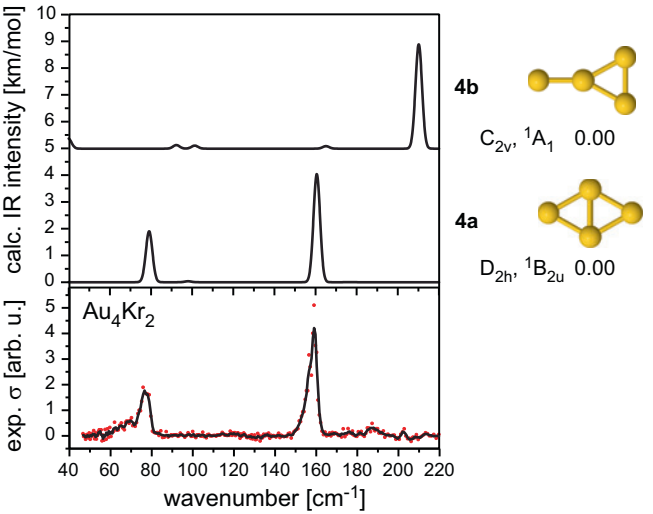

Figure 4: Comparison of the IR-MPD spectrum of Au_4Kr_2 with calculated spectra for low energy isomers of Au_4. Relative energies of the isomers are given in eV and include zero point vibrational energy corrections. The calculated line spectra are folded with a Gaussian line-width function of 3 cm^{-1} full width at half maximum for better visual comparison with the experimental spectra.

bands at 76 cm^{-1} (calc.: 78.5 cm^{-1}) and 158 cm^{-1} (159.1 cm^{-1}), attributed to the **4a** isomer, are in-plane vibrations of the central Au-dimer against the outer two atoms.

The here not observed Y-isomer can be formed by photodetachement from anionic Au_4^- that is known to have this shape [56]. Using vibrationally resolved photoelectron spectroscopy the frequencies of three vibrational modes at 17(7), 97(7), and 171(7) cm^{-1} of the resulting neutral have been determined and assigned to this Y-isomer [40]. We also observe good agreement with the values obtained for isomer **4b** at the TPSS/def2-TZVP level of theory (14.4 cm^{-1} b_2; 91.6 cm^{-1} a_1; 164.8 cm^{-1} a_1).

3.4 Au_5

The far-IR-MPD spectrum of Au_5Kr has an unfavourable signal-to-noise ratio (cf. the comparison with the other IR-MPD spectra in Figure 3) and the bands are not very pronounced. This may be related to the low intensity of the species in the mass spectrum. Comparison with calculated spectra (Figure 5) shows that the

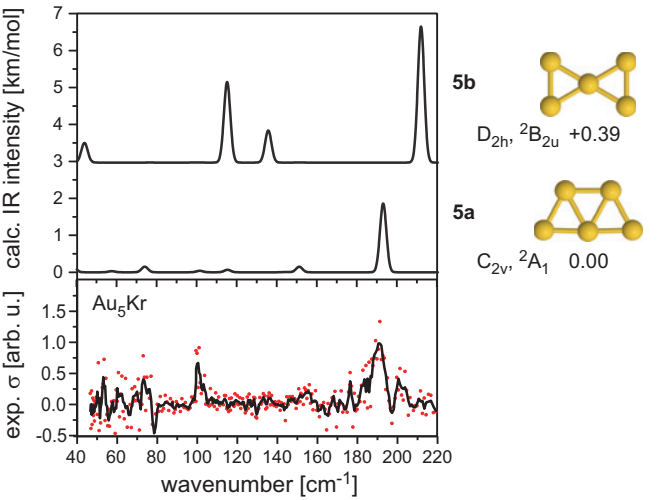

Figure 5: Comparison of the IR-MPD spectrum of Au_5Kr with calculated spectra for low energy isomers of Au_5. Relative energies of the isomers are given in eV and include zero point vibrational energy corrections.

only definite band in the experimental spectrum at 192 cm^{-1} coincides with the most intense and highest frequency mode at 192.1 cm^{-1} of the calculated ground state isomer **5a**, a planar trapezoidal structure (Figure 5). The presence of the X-shaped isomer can be excluded as it does not fit the experimental spectrum and it is significantly higher in energy.

3.5 Au_6

For Au_6, no experimental data is available. The mass spectrum contains no signals for this cluster size, neither for the bare cluster, nor for its krypton complexes. This can be attributed to the very high ionization potential of this cluster, which is measured to be 8.8 eV [29] and thus well above the photon energy used here for ionization (7.8 eV). The predicted ground state structure is a planar triangle (D_{3h}, $^1E'$).

3.6 Au_7

The IR-MPD spectrum of the 7-atom cluster has been discussed before, and it has been shown that its structure is a planar triangle with an additional atom

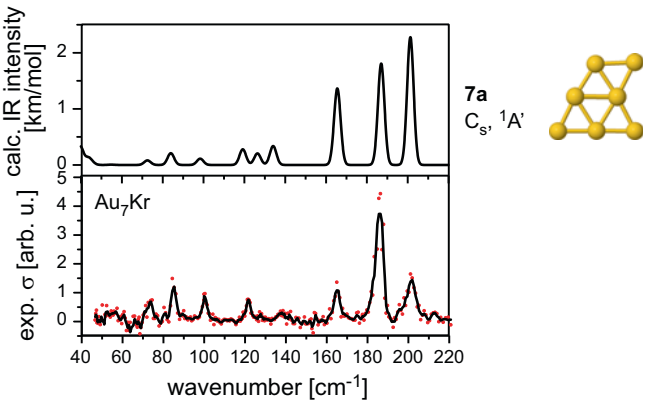

Figure 6: Comparison of the IR-MPD spectrum of Au_7Kr with the calculated spectrum of the ground state isomer of Au_7.

bound to one of its edges [10, 11]. The harmonic spectrum shown in Figure 6 is in good agreement with the experimental multiple photon dissociation spectrum of Au_7Kr. However, some deviations in the band intensities and a slight broadening of the experimentally determined highest frequency bands can be noted. It has been suggested that these effects are related to the rare gas binding [10, 57], but recent calculations explicitly considering dispersion interactions, find that they are due to anharmonic effects caused by the fluctional behaviour at the experimental temperature [11]. Modelling of the finite temperature IR spectrum *via* molecular dynamics simulations can well explain the experimental features. At elevated temperatures, the dynamics involves self-isomerization *via* the C_{2v} symmetric structure of the anion into a geometry equivalent to the starting structure.

3.7 Au_8

In the following, only the experimental spectrum of Au_8Kr_3 is discussed, as it is very similar to the spectrum of Au_8Kr_2 but has a slightly better quality. It shows the onset of a band at the low-frequency end of the spectrum (~ 46 cm^{-1}) as well as two rather pronounced lines at 113 cm^{-1} and 193 cm^{-1}. As seen in Figure 7, this agrees well with the calculated band positions (42.2, 110.7, 194.6 cm^{-1}) for the planar star-shaped D_{4h} ground state geometry **8a**, although the relative intensity of the second band is significantly too low in the computed spectrum. This might be an anharmonic effect or due to the influence of the rare gas atoms. In the Kr complexes, the symmetry is reduced, which may lead to splitting of degenerate modes

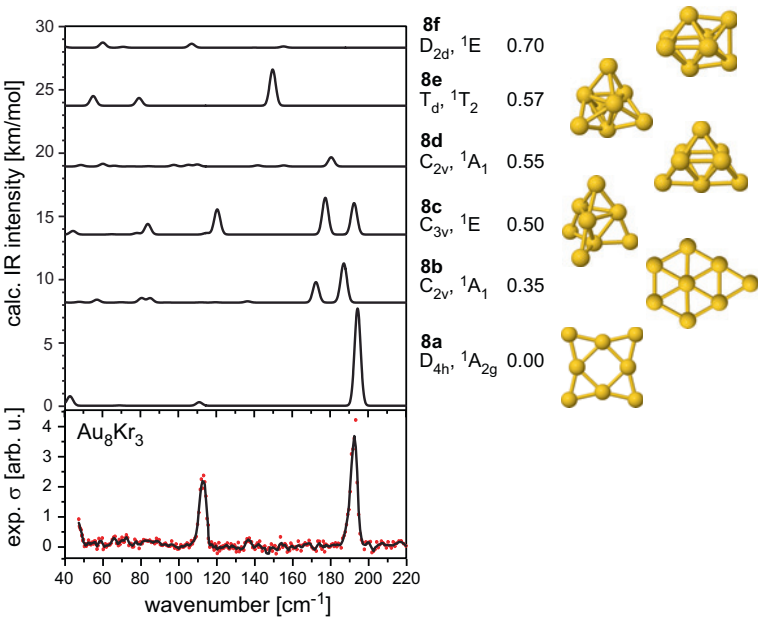

Figure 7: Comparison of the IR-MPD spectrum of Au_8Kr_3 with calculated IR spectra of low energy isomers of Au_8. All calculated spectra are plotted on the same intensity scale, but offset for clarity. Relative energies of the isomers are given in eV and include zero-point vibrational energy corrections.

(not observed here) or the appearance of bands that are initially not IR-allowed. The latter may be the case for the small feature in the experimental spectrum at 137 cm^{-1} that fits well to an IR-inactive mode at 136.2 cm^{-1} in the **8a** structure. A second planar isomer **8b** and all 3D-structures **8c-f** are significantly higher in energy and do not match the experimental IR spectrum. While inclusion of dispersion forces in the calculations is expected to lower the relative energies of the 3D isomers, the assignment to the planar star-shaped D_{4h} structure is unambiguous.

4 Conclusions

The far-IR spectra of small neutral gold clusters complexed with krypton atoms Au_nKr_m ($n = 3$–5, 7, 8) are presented. For $n = 5, 7, 8$ the comparison with calculated harmonic spectra of the bare Au_n clusters results in good agreement for the lowest energy isomers at the TPSS/def2-TZVP level of theory. In the case of Au_4, the

assigned structure is one of two calculated isoenergetic lowest-energy isomers, while the second one is not observed, possibly due to its higher ionization energy. The second isomer is found to be formed *via* electron detachment from anionic Au_4^- [40]. All of the identified structures are fully planar, showing that, contrary to some theoretical predictions, neutral gold clusters remain 2-dimensional until at least Au_8. While rare gas binding and anharmonicity effects can have an influence on the observed far-IR spectra of Au_nKr_m [11, 57], for the sizes discussed here, unambiguous assignment is possible by considering the harmonic vibrational spectra of the bare Au_n.

5 Supplementary information

Cartesian coordinates of the gold cluster structures and (unscaled) vibrational frequencies of all isomers.

Acknowledgement: We gratefully acknowledge the "Stichting voor Fundamental Onderzoek der Materie" (FOM) in providing beam time on FELIX and the skilful assistance of the FELIX staff, in particular A. F. G. van der Meer and B. Redlich. This work is supported by the Cluster of Excellence "Unifying Concepts in Catalysis" coordinated by the Technical University Berlin and funded by the Deutsche Forschungsgemeinschaft (DFG). J. T. L. acknowledges support from the Alexander-von-Humboldt-Stiftung. We thank G. Meijer for his continued support.

Received November 1, 2013; accepted December 17, 2013.

References

1. K. Rademann, Ber. Bunsenges. Phys. Chem. **93** (1989) 653.
2. B. V. Issendorff and O. Cheshnovski, Annu. Rev. Phys. Chem. **56** (2005) 549.
3. M. Eichelbaum, K. Rademann, R. Müller, M. Radtke, H. Riesemeier, and W. Görner, Angew. Chem. Int. Edit. **44** (2005) 7905.
4. M. Eichelbaum, K. Rademann, A. Hoell, D. M. Tatchev, W. Weigel, R. Stößer, and G. Pacchioni, Nanotechnology **19** (2008) 135701.
5. M. Haruta, T. Kobayashi, H. Sano, and N. Yamada, Chem. Lett. **16** (1987) 405.
6. T. M. Bernhardt, Int. J. Mass Spectrom. **243** (2005) 1.
7. D. Schooss, P. Weis, O. Hampe, and M. M. Kappes, Philos. T. R. Soc. A **368** (2010) 1211.
8. L.-M. Wang and L.-S. Wang, Nanoscale **4** (2012) 4038.

9. A. P. Woodham and A. Fielicke, in: *Structure & Bonding: Gold Clusters, Colloids and Nano-Particles*, D. M. P. Mingos (Ed.), Springer, Berlin, in press, DOI: 10.1007/430_2013_136.
10. P. Gruene, D. M. Rayner, B. Redlich, A. F. G. van der Meer, J. T. Lyon, G. Meijer, and A. Fielicke, Science **321** (2008) 674.
11. L. M. Ghiringhelli, P. Gruene, J. T. Lyon, D. M. Rayner, G. Meijer, A. Fielicke, and M. Scheffler, New J. Phys. **15** (2013) 083003.
12. G. Bravo-Pérez, I. L. Garzón, and O. Novaro, J. Mol. Struc. THEOCHEM **493** (1999) 225.
13. H. Grönbeck and W. Andreoni, Chem. Phys. **262** (2000) 1.
14. V. Bonacic-Koutecký, J. Burda, R. Mitric, M. Ge, G. Zampella, and P. Fantucci, J. Chem. Phys. **117** (2002) 3120.
15. E. M. Fernández, J. M. Soler, , I. L. Garzón, L. C. Balbás, Phys. Rev. B **70** (2004) 165403.
16. F. Remacle and E. S. Kryachko, J. Chem. Phys. **122** (2005) 044304.
17. B. Assadollahzadeh and P. Schwerdtfeger, J. Chem. Phys. **131** (2009) 064306.
18. H. M. Lee and K. S. Kim, Chem. Eur. J. **18** (2012) 13203.
19. D. A. Götz, R. Schäfer, and P. Schwerdtfeger, J. Comput. Chem. **34** (2013) 1975.
20. H. Häkkinen and U. Landman, Phys. Rev. B **62** (2000) R2287.
21. J. Wang, G. Wang, and J. Zhao, Phys. Rev. B **66** (2002) 035418.
22. R. M. Olson, S. Varganov, M. S. Gordon, H. Metiu, S. Chretien, P. Piecuch, K. Kowalski, S. A. Kucharski, and M. Musial, J. Am. Chem. Soc. **127** (2005) 1049.
23. H. Grönbeck and P. Broqvist, Phys. Rev. B **71** (2005) 073408.
24. Y.-K. Han, J. Chem. Phys. **124** (2006) 024316.
25. M. Diefenbach and K. S. Kim, J. Phys. Chem. B **110** (2006) 21639.
26. R. M. Olson and M. S. Gordon, J. Chem. Phys. **126** (2007) 214310.
27. S. A. Serapian, M. J. Bearpark, and F. Bresme, Nanoscale **5** (2013) 6445.
28. J. A. Hansen, P. Piecuch, and B. G. Levine, J. Chem. Phys. **139** (2013) 091101.
29. C. Jackschath, I. Rabin, and W. Schulze, Ber. Bunsenges. Phys. Chem. **96** (1992) 1200.
30. G. A. Bishea and M. D. Morse, J. Chem. Phys. **95** (1991) 8779.
31. R. Guo, K. Balasubramanian, X. Wang, and L. Andrews, J. Chem. Phys. **117** (2002) 1614.
32. B. A. Collings, K. Athanassenas, D. Lacombe, D. M. Rayner, and P. A. Hackett, J. Chem. Phys. **101** (1994) 3506.
33. S. Lecoultre, A. Rydlo, C. Felix, J. Buttet, S. Gilb, and W. Harbich, J. Chem. Phys. **134** (2011) 074302.
34. J. Ho, K. M. Ervin, and W. C. Lineberger, J. Chem. Phys. **93** (1990) 6987.
35. G. F. Gantefor, D. M. Cox, and A. Kaldor, J. Chem. Phys. **93** (1990) 8395.
36. G. F. Gantefor, D. M. Cox, and A. Kaldor, J. Chem. Phys. **96** (1992) 4102.
37. H. Handschuh, G. Ganteför, and W. Eberhardt, Rev. Sci. Instrum. **66** (1995) 3838.
38. D. M. Neumark, J. Phys. Chem. A **112** (2008) 13287.
39. I. León, Z. Yang, and L.-S. Wang, J. Chem. Phys. **138** (2013) 184304.
40. Z. Yang, I. León, and L.-S. Wang, J. Chem. Phys. **139** (2013) 021106.
41. D. Oepts, A. F. G. van der Meer, and P. W. van Amersfoort, Infrared Phys. Techn. **36** (1995) 297.
42. A. Fielicke, A. Kirilyuk, C. Ratsch, J. Behler, M. Scheffler, G. von Helden, and G. Meijer, Phys. Rev. Lett. **93** (2004) 023401.
43. A. Fielicke, G. von Helden, and G. Meijer, Eur. Phys. J. D **34** (2005) 83.
44. R. Campargue, Rev. Sci. Instrum. **35** (1964) 111.
45. A. Fielicke and K. Rademann, J. Phys. Chem. A **104** (2000) 6979.
46. R. Ahlrichs, M. Bär, M. Häser, H. Horn, and C. Kölmel, Chem. Phys. Lett. **162** (1989) 165.

47. F. Weigend and R. Ahlrichs, Phys. Chem. Chem. Phys. **7** (2005) 3297.
48. J. Tao, J. P. Perdew, V. N. Staroverov, and G. E. Scuseria, Phys. Rev. Lett. **91** (2003) 146401.
49. M. P. Johansson, A. Lechtken, D. Schooss, M. M. Kappes, and F. Furche, Phys. Rev. A **77** (2008) 053202.
50. M. Mantina, R. Valero, and D. G. Truhlar, J. Chem. Phys. **131** (2009) 064706.
51. R. J. Meier, Vib. Spectrosc. **43** (2007) 26.
52. J. P. Merrick, D. Moran, and L. Radom, J. Phys. Chem. A **111** (2007) 11683.
53. J. T. Lyon, P. Gruene, A. Fielicke, G. Meijer, E. Janssens, P. Claes, and P. Lievens, J. Am. Chem. Soc. **131** (2009) 1115.
54. V. T. Ngan, P. Gruene, P. Claes, E. Janssens, A. Fielicke, M. T. Nguyen, and P. Lievens, J. Am. Chem. Soc. **132** (2010) 15589.
55. M. B. Knickelbein and W. J. C. Menezes, Chem. Phys. Lett. **184** (1991) 433.
56. F. Furche, R. Ahlrichs, P. Weis, C. Jacob, S. Gilb, T. Bierweiler, and M. M. Kappes, J. Chem. Phys. **117** (2002) 6982.
57. L. A. Mancera and D. M. Benoit, Phys. Chem. Chem. Phys. **15** (2013) 1929.